HHS Public Access

Author manuscript

Glia. Author manuscript; available in PMC 2018 September 01.

Published in final edited form as:

Glia. 2017 September ; 65(9): 1535–1549. doi:10.1002/glia.23180.

TRPC1- and TRPC3-dependent Ca^{2+} signaling in mouse cortical astrocytes affects injury-evoked astrogliosis *in vivo*

Thabet Belkacemi[a], **Alexander Niermann**[a], **Laura Hofmann**[a], **Ulrich Wissenbach**[a], **Lutz Birnbaumer**[e], **Petra Leidinger**[c], **Christina Backes**[f], **Eckart Meese**[c], **Andreas Keller**[f], **Xianshu Bai**[d], **Anja Scheller**[d], **Frank Kirchhoff**[d], **Stephan E. Philipp**[a], **Petra Weissgerber**[a], **Veit Flockerzi**[a], and **Andreas Beck**[a,b]

[a]Experimentelle und Klinische Pharmakologie und Toxikologie, Universität des Saarlandes, 66421 Homburg, Germany

[b]Zentrum für Human- und Molekularbiologie, Universität des Saarlandes, 66421 Homburg, Germany

[c]Institut für Humangenetik, Universität des Saarlandes, 66421 Homburg, Germany

[d]Molekulare Physiologie, Universität des Saarlandes, 66421 Homburg, Germany

[e]Neurobiology Laboratory, National Institute of Environmental Health Sciences, Research Triangle Park, North Carolina 27709, USA and Institute of Biomedical Research (BIOMED), Catholic University of Argentina, Buenos Aires C1107AFF, Argentina

[f]Klinische Bioinformatik, Universität des Saarlandes, 66123 Saarbrücken, Germany

Abstract

Following brain injury astrocytes change into a reactive state, proliferate and grow into the site of lesion, a process called astrogliosis, initiated and regulated by changes in cytoplasmic Ca^{2+}. Transient receptor potential canonical (TRPC) channels may contribute to Ca^{2+} influx but their presence and possible function in astrocytes is not known. By RT-PCR and RNA sequencing we identified transcripts of *Trpc1*, *Trpc2*, *Trpc3* and *Trpc4* in FACS-sorted glutamate aspartate transporter (GLAST)-positive cultured mouse cortical astrocytes and subcloned full-length *Trpc1* and *Trpc3* cDNAs from these cells. Ca^{2+} entry in cortical astrocytes depended on TRPC3 and was increased in the absence of *Trpc1*. After co-expression of *Trpc1* and *Trpc3* in HEK-293 cells both proteins co-immunoprecipitate and form functional heteromeric channels, with TRPC1 reducing TRPC3 activity. *In vitro*, lack of *Trpc3* reduced astrocyte proliferation and migration whereas the TRPC3 gain-of-function moonwalker mutation and *Trpc1* deficiency increased astrocyte

Correspondence should be addressed to: Andreas Beck, Experimentelle und Klinische Pharmakologie und Toxikologie, Universität des Saarlandes, 66421 Homburg, Germany; Tel.: +49 6841 1626422; andreas.beck@uniklinikum-saarland.de.

Authors contributions

T.B. designed and performed experiments and analyzed the data; A.N. and T.B. performed proliferation and migration assays; L.H., U.W. and T.B. performed Co-IPs and Western Blots; S.E.P. performed FACS; X.B. and A.S. performed initial stab wound experiments together with T.B.; E.M., P.L., C.B. and A.K. provided transcriptome and microarray data; L.B. provided mice; P.W. performed embryo transfer and mouse breeding; F.K., T.B. and V.F. edited the manuscript; A.B. conceived and designed the experiments, directed the project, analyzed data and wrote the manuscript.

Competing financial interests

The authors declare no competing financial interests.

migration. *In vivo*, astrogliosis and cortex edema following stab wound injury were reduced in *Trpc3*$^{-/-}$ but increased in *Trpc1*$^{-/-}$ mice. In summary, our results show a decisive contribution of TRPC3 to astrocyte Ca^{2+} signaling, which is even augmented in the absence of *Trpc1*, in particular following brain injury. Targeted therapies to reduce TRPC3 channel activity in astrocytes might therefore be beneficial in traumatic brain injury.

Keywords

glia; membrane currents; ion channels; proliferation; migration; stab wound injury

Introduction

The incidence of acute traumatic brain injuries (TBIs) was estimated to be 235 per 100,000 per year with a mortality rate of 15 per 100,000 per year in Europe (Tagliaferri, Compagnone, Korsic, Servadei, & Kraus, 2006). In the United States annually an estimated 1,7 million people sustain a TBI, with 52,000 people dying from their injury (Faul, Xu, Wald, Coronado, & Dellinger, 2010). TBIs are followed by changes in cerebral blood flow, inflammation, alterations in oxygen delivery and metabolism and death of neural cells (Dutton & McCunn, 2003). Damaged tissue, blood components and diverse messenger molecules activate astrocytes into a reactive state, called astrogliosis, accompanied by increased proliferation and growth towards the lesion (Bardehle et al., 2013; Sofroniew, 2009). The activated astrocytes then generate a glial scar, which is beneficial in covering the damaged area, but hampers axonal regeneration (Windle, Clemente, & Chambers, 1952). Thus, astrocytes can be both protective and hazardous to neurons, and manipulating their function might be a valuable strategy for neuroprotection and regeneration after TBI. Cell proliferation, growth and migration are among the cellular functions controlled by cytoplasmic Ca^{2+}, which is either released from intracellular stores after stimulation of Gq protein-coupled receptors or receptor tyrosine kinases, or enters the cell via Ca^{2+}-permeable ion channels in the plasma membrane. Canonical transient receptor potential (TRPC) channels may contribute to the Ca^{2+} influx mediating proliferation, growth and migration of various cell types (Deliot & Constantin, 2015; Kuang et al., 2012; Zhao et al., 2012) including astrocytes.

It has been shown that astrocytoma cells and astrocytes from different preparations express diverse *Trpc* transcripts, including *Trpc1* (Akita & Okada, 2011; Golovina, 2005; Li et al., 2011; Malarkey, Ni, & Parpura, 2008; Reyes, Verkhratsky, & Parpura, 2013), *Trpc3* (Akita & Okada, 2011; Grimaldi, Maratos, & Verma, 2003; Miyano et al., 2010; Munakata et al., 2013; Shirakawa et al., 2010; Streifel et al., 2014; Streifel, Miller, Mouneimne, & Tjalkens, 2013), *Trpc4* (Song et al., 2005), *Trpc5* (Malarkey et al., 2008) and *Trpc6* (Beskina, Miller, Mazzocco-Spezzia, Pulina, & Golovina, 2007), and that TRPC1 is important for proliferation and chemotactic migration of human malignant glioma (astrocytoma) cells (Bomben & Sontheimer, 2010; Bomben, Turner, Barclay, & Sontheimer, 2011), but there are very few studies correlating TRPC activity with astrocyte function *in vitro* and *in vivo*.

In this study we wanted to identify *Trpc* expression in cortical astrocytes and to characterize the role of TRPCs for astrocyte function *in vitro* and, in a defined stab wound injury model, *in vivo*. With very few exceptions no specific agonists or antagonists are available for TRPC channels which would allow for specifically isolating TRPC currents and Ca^{2+} signals. Therefore, we made use of genetically modified mice with *Trpc1* and *Trpc3* deficiencies and mice harboring a heterozygous gain-of-function mutation within *Trpc3*, the moonwalker (mwk) mice (Becker, 2014; Becker et al., 2009). For *in vitro* studies cortical astrocytes from these mice were cultured to compare TRPC-dependent Ca^{2+} signaling. To prepare RNA to perform PCR and next generation sequencing we used pure GLAST-positive astrocytes sorted by FACS to avoid contribution of other cell types. We show, that i) TRPC3 and TRPC1 are present in cortical astrocytes, that ii) TRPC3 promotes astrocyte proliferation and migration *in vitro* as well as iii) astrogliosis and cortical edema after cortical stab wound injury in mice *in vivo*, whereas iv) TRPC1 significantly mitigates these TRPC3 activities.

Materials and Methods

Mice

Trpc1$^{-/-}$ (Dietrich et al., 2007), *Trpc3*$^{-/-}$ (Hartmann et al., 2008), *Trpc6*$^{-/-}$ (Tsvilovskyy et al., 2009) and *Trpc3*$^{-/-}$/*Trpc6*$^{-/-}$ (Quick et al., 2012) as well as heterozygous $TRPC3_{T635A}$ mutant moonwalker (mwk) mice (Becker et al., 2009) were kept in a specific pathogen-free animal facility and bred to a C57BL6/N or 129SvJ/C57Bl6/N background. *Trpc1*$^{-/-}$/*Trpc*5$^{-/-}$ and *Trpc3*$^{-/-}$/*Trpc6*$^{-/-}$ mice were generated by crossing the single gene-deficient strains. The heterozygous $TRPC3_{T635A}$ mutant mwk mouse was purchased from Harwell Science and Innovation (Harwell, Oxfordshire, UK) and embryo-transferred into our mouse facility. All animal experiments were performed in accordance with the German legislation on the protection of animals and were approved by the responsible local ethics committee (AZ C1-2.4.2.2/11-2015).

Preparation and culture of mouse cortical astrocytes

Newborn (0–3 days) mice were decapitated. The cerebral cortices were isolated in ice cold PBS and the meninges were removed. The tissues were incubated with trypsin (5 g/l, Sigma) for 15 min at 37°C and digestion was stopped by adding Dulbecco´s Modified Eagle Medium (DMEM, Fisher Scientific) supplemented with 10% fetal calf serum (FCS, Fisher Scientific). The cortices were then triturated by pipetting up and down (10 times) using a 20G needle. The obtained suspension was filtered through a 40 μm cell strainer (BD Falcon) and centrifuged for 5 min at 200 g. Cells were re-suspended in DMEM containing 10% FCS, 1% GlutaMAX, 100 U/ml Penicillin and 100 μg/ml Streptomycin, plated in 75 cm^2 poly-L-lysine (PLL, 0.1 mg/ml, Sigma) -coated flasks (BD Falcon; 3 brains per flask) and cultured at 37°C and 5% CO_2 in a humidified incubator. After 2 to 3 days, the medium was changed to remove dead cells and debris. Afterwards the medium was changed twice a week until the cells reached confluency. For experiments microglial cells were removed by shaking, and astrocytes were trypsinized and subcultured either in 96-well plates for proliferation assays, 6-well plates for migration and proliferation assays or on PLL-coated glass coverslips for Ca^{2+} imaging or patch clamp experiments.

Cell lines and transfection

HEK-293 cells (ATCC, CRL 1573) were obtained from the American Type Culture Collection (Manassas, VA, USA). HEK cells stably expressing the human *Trpc3* cDNA (Zhu, Jiang, & Birnbaumer, 1998) were kindly provided by Dr. M.X. Zhu (University of Texas Health Science Center, Houston, US). HEK cells stably expressing the mouse *Trpc1* cDNA (accession no. NM-011643.3) or the tetracycline-inducible mouse moonwalker $Trpc3_{T635A}$ cDNA were generated as described (Beck et al., 2013). For the latter, nucleotide A at position 1903 was replaced by G in the mouse *Trpc3* cDNA (accession no. NM_019510) and the cDNA was subcloned into the pCDNA5/FRT/TO vector (Invitrogen). Cells were induced with 1 μg/ml tetracycline 2 h before the experiments, resulting in a strong expression of the mwk TRPC3. Wild-type HEK cells were cultured in Minimal Essential Medium (MEM, Fisher Scientific) and all other HEK cell lines in DMEM, supplemented with 10% FCS. Cells were kept in an incubator at 37°C and 5% CO_2, and the medium was changed twice a week.

For Ca^{2+} imaging and patch clamp experiments cells were plated on glass coverslips coated with PLL. For transfection, HEK cells were cultured in 3.5 mm petri dishes until reaching 70% confluency and medium was renewed prior to transfection. The transfection mixture was prepared following the manufacturer`s recommendation using FuGENE HD Transfection Reagent (Promega). For every 3.5 mm petri dish, 2 μg of cDNA was mixed with 5 μl of FuGENE HD reagent and 100 μl of Opti-MEM medium (Thermo Scientific) and incubated at room temperature for 15 min. The transfection mixture was added onto the cells and incubated at 37°C and 5% CO_2 for 48 h. Then, cells were plated on PLL-coated glass coverslips and used for experiments for the next 24 h.

Co-immunoprecipitation and western blot

Co-immunoprecipitation, SDS-Page and western blots were performed as described previously (Zimmermann et al., 2014) using antibodies for mouse TRPC3 (ab 45/47 and ab 1378), mouse TRPC1 (F2-E4) and mouse Cavβ3 (ab 828), all generated in-house. To quantify the expression of glial fibrillary acidic protein (GFAP) after stab wound injury (see below), we analyzed the injured cortical hemispheres from fixed brain slices of wild-type and $Trpc3^{-/-}$ mice. Total protein was extracted from the fixed brain slices using Qproteome FFPE Tissue Kit (Qiagene) according to the manufacturer´s guidelines and western blots were performed using antibodies for GFAP (rabbit anti-GFAP, 1:5000, SYnaptic SYstems) and α-tubulin (mouse anti-α-tubulin, 1:200, Santa Cruz Biotechnology). Proteins were detected with horse-radish peroxidase-coupled secondary antibodies and Western Lightning Chemiluminescence Reagent Plus (PerkinElmer Life Sciences). Original scans were saved as TIFF files from LAS 3000 (Fujifilm), which were further processed in Adobe Photoshop or Corel Draw. Images were cropped, resized proportionally, and brought to the resolution required for publication. To quantify GFAP, the background signals of the western blots were subtracted and the intensity of the GFAP staining was normalized to the corresponding intensity of the α-tubulin staining.

Preparative fluorescence-activated cell sorting (FACS)

2 to 3 weeks after preparation cortical cultures were trypsinized and suspended into culture medium, washed with phosphate-buffered saline (PBS) and re-suspended in 0.5% BSA in PBS buffer. Cells were incubated at 4°C for 10 min with anti-GLAST-PE (1:10, Miltenyi Biotec) and anti-CD11b-FITC (1:10, Miltenyi Biotec) in 0.5% BSA in PBS, and afterwards washed with 0.5% (w/v) bovine serum albumin (BSA, Sigma) in PBS, and loaded directly into the FACS (MoFlo, Beckman Coulter). 100 GLAST-positive CD11b-negative astrocytes or 50 GLAST-negative CD11b-positive microglial cells were sorted per RNase-free PCR tube. For RNA sequencing and microarray transcriptome analysis all cells from a culture flask were sorted in one vial. The tubes were immediately placed into liquid nitrogen and transferred to a −80°C freezer until further use.

RT-PCR

One-step RT-PCR was performed on 100 sorted GLAST-positive astrocytes and 50 sorted CD11b-positive microglial cells using SuperScript™ One-Step RT-PCR with Platinum Taq (Invitrogen). Each 25 µl reaction contained 0.5 µl sorted cells, 12.5 µl 2x Reaction Mix (0.4 mM dNTP, 24 mM $MgSO_4$), 0.5 µl RT/Platinum Taq DNA Polymerase, 0.75 µl forward primer (10 pmol/µl), 0.75 µl reverse primer (10 pmol/µl) and 10 µl sterile deionized H_2O. Cycle protocol: 30 min 50°C, 2 min 94°C, 60 cycles of 15 s 94°C + 15 s 62°C + 20 s (from the 16^{th} cycle the time was increased by 2 s per cycle) 70°C, 5 min 72°C, 4°C.

Full length *Trpc1* and *Trpc3* cDNAs were amplified from sorted astrocytes as follows: Total RNA was extracted from GLAST-positive sorted astrocytes using RNeasy Mini Kit (Qiagen) and first strand cDNA was synthetized using the Maxima first strand cDNA synthesis kit (Thermo Scientific). The PCR was performed using KOD Xtreme™ Hot Start DNA Polymerase (Merck Millipore). Every reaction contained 25 µl of PCR mix (3 µl cDNA (obtained from reverse transcription of 734.51 ng of RNA), 12.5 µl 2x Xtreme™ Buffer, 5 µl dNTPs (0.4 mM), 2 × 0.75 µl primers (10 pmol/µl each), 2.5 µl H_2O and 0.5 µl KOD-Xtreme™ polymerase (1 U/µl)). Cycle protocol: 2 min 94°C, 40 cycles of 10 s 98°C + 30 s 62°C + 3 min 68°C, 5 min 68°C, 4°C. The amplified cDNAs were subcloned into pUC19 and sequenced on both strands. Table 1 shows the primers used for PCR.

Next generation sequencing

RNA probes from three independent astrocyte cultures were sequenced (paired-end, 75 bp) using an Illumina HiSeq sequencing system (Illumina Inc., San Diego, CA, US). Raw data were mapped against the mouse genome NCBI/build37.2 using TopHat (Trapnell, Pachter, & Salzberg, 2009). For the detection of differentially expressed genes and transcripts we followed the protocol of Trapnell et al. (Trapnell et al., 2012) closely using the tool Cuffdiff.

Oligonucleotide microarray analysis

The mRNA of probes from three independent astrocyte cultures each isolated from wild-type and *Trpc3*$^{-/-}$ mice were analyzed by Agilent. In brief, the raw intensity values were extracted from the image file using feature extraction software (Agilent Technologies). We used the *gMedianSignal* values as expression values for the probes and summarized the

probes belonging to the same transcript by taking the median of these values. We applied quantile normalization before using the expression values in downstream analysis.

Calcium Imaging

Astrocytes and HEK cells plated on PLL-coated glass coverslips were loaded with 5 μM Fura-2-AM in medium in the dark at 37°C for 30 to 40 min, then washed with bath solution (in mM: 140 NaCl, 4 KCl, 1 $MgCl_2$, 2 $CaCl_2$, 10 HEPES, 10 glucose, pH adjusted to 7.2 with NaOH). For nominal Ca^{2+}-free solution $CaCl_2$ was replaced by $MgCl_2$. Measurements were performed on a monochromator (Polychrome V, TILL-Photonics) -equipped inverted microscope (Axiovert S100, Zeiss) using a 20x Fluar objective (Zeiss). Every 2 s Fura-2 was alternately excited at 340 nm and 380 nm for 30 ms each and the emitted fluorescence (F340 and F380, >510 nm) were recorded with a cooled charge-coupled device (CCD) camera (TILL Imago, TILL-Photonics, Germany). Ratio images were calculated from F340 and F380 pictures after background correction i.e. subtraction of the fluorescence intensity at 340 and 380 nm excitation from a cell-free area. Single cells were marked as regions of interest and F340/F380 was plotted versus time. Monochromator, camera, acquisition and analysis were controlled by TILLvisION software (TILL-Photonics).

Electrophysiological recordings

Membrane currents were recorded in the tight seal whole-cell patch clamp configuration using an EPC-9 amplifier (HEKA Electronics, Lambrecht, Germany). Patch pipettes were pulled from glass capillaries GB150T-8P (Science Products, Hofheim, Germany) at a vertical Puller (PC-10, Narishige, Tokyo, Japan) and had resistances between 2 and 4 MΩ when filled with standard internal solution (in mM: 140 Cs-methanesulfonate, 8 NaCl, 1 $MgCl_2$, 10 HEPES, 10 Cs-BAPTA, 3.1 $CaCl_2$ (100 nM free Ca^{2+}, calculated with WebMaxC http://www.stanford.edu/~cpatton/webmaxcS.htm) pH adjusted to 7.2 with CsOH. For Ca^{2+}-free intracellular solution $CaCl_2$ was omitted. The compounds used for external application were diluted into the extracellular solution (in mM: 140 NaCl, 2 $MgCl_2$, 1 $CaCl_2$, 10 HEPES, 10 glucose, pH adjusted to 7.2 with NaOH) to achieve the final concentration as indicated. For nominal Ca^{2+}-free solution $CaCl_2$ was replaced by $MgCl_2$. All modified solutions were directly applied onto the patch-clamped cell via an air pressure-driven (MPCU, Lorenz Meßgerätebau, Katlenburg-Lindau, Germany) application pipette. Osmolality of all solutions ranged from 290 to 310 mOsm. Voltage ramps of 400 ms duration spanning a voltage range from −100 mV to +100 mV were applied every 2 s from a holding potential (V_h) of 0 mV using the PatchMaster software (HEKA). All voltages were corrected for a 10 mV liquid junction potential. Currents were filtered at 2.9 kHz and digitized at 400 μs intervals. Capacitive currents and series resistance were determined and corrected before each voltage ramp using the automatic capacitance compensation of the EPC-9. Inward and outward currents were extracted from each individual ramp current recording by measuring the current amplitudes at −80 and +80 mV, respectively, and plotted versus time. Basal currents before an application were subtracted to get the net developing current. Current-voltage (IV) relationships were extracted at indicated time points. Currents were normalized to the initial size i.e. capacitance of the cell to obtain current densities (pA/pF).

Expansion/Migration Assay

The expansion and migration of astrocytes was studied using a scratch assay in which expansion and migration of cells was assessed by the rate of recovery of a defined scratched area on a confluent cell layer. Cells were plated in PLL-coated 6-well plates scratched from the outside bottom as markers to find the exact same regions for analysis again. Once cells reached confluency, two scratches were performed in every well (vertical to the outside bottom scratch) using a 200 µl pipette tip. Wells were washed with PBS to remove the detached cells and incubated at 37°C 5% CO_2 without FCS to inhibit proliferation. At 0, 4, 8 and 24 hours four pictures per well were taken at the crossing between the cellular scratch and the outside bottom marker scratch, using a phase-contrast light microscope (Axiovert 40C, Zeiss) equipped with a 10x A-Plan objective (Zeiss) and a camera (AxioCam, Zeiss). Expansion and migration were quantified as the average of the cell-free scratch area reoccupied by the recruited cells using Image J software (NIH). All measured areas were normalized to the “0 hour” area (100% cell-free scratch area).

Proliferation Assay

Astrocytes proliferation was quantified using the colorimetric MTS cell proliferation assay (Promega). 5000 cells per well were plated in a 96-well plate in triplicate and incubated at 37°C with medium containing 10% FCS. The amount of viable cells was determined after incubating the desired wells with 20 µl of MTS for 1 hour at 37°C by measuring the absorbance of the MTS metabolite formazan at 490 nm using a 96-well plate reader (infinite M200 TECAN). Measurements were performed at day 0 (right after plating), 3, 5, 6 and 7. The absorbance of the medium was subtracted as background.

The proliferative activity of astrocytes after injury was studied by performing a scratch assay (see above). Cells were plated on PLL-coated glass coverslips in 24-well plates and after reaching confluency, scratches were made using a 200 µl pipette tip. Coverslips were washed with PBS to remove the detached cells and incubated at 37°C 5% CO_2 in DMEM with 10% FCS. After 24 h cells were fixed and incubated with 4′6-diamidino-2-phenylindole (DAPI, Sigma Aldrich) and rabbit anti-Ki-67 antibody (1:200, Thermo Fisher Scientific), a cellular marker for proliferation. The anti-Ki-67 antibody was stained by a donkey anti-rabbit Alexa 555 antibody (1:500, Invitrogen). Images were taken at a fluorescent microscope (Zeiss Axio Scan.Z1) equipped with the appropriate filter sets. The Ki-67-positive cells were counted in a defined area around the scratch and normalized to the total number of cells.

Cortical stab wound and immunohistochemistry

8 and 11 week-old male *Trpc3*$^{-/-}$ and *Trpc1*$^{-/-}$/*Trpc5*$^{-/-}$ mice, respectively, and their corresponding wild-type mice, were anaesthetized using ketamine (87 mg/kg body weight) and xylazine (13 mg/kg body weight) via intraperitoneal injection and placed on a stereotactic instrument. A 1 cm long incision in the skin was made and, using an electric drill, the skull was thinned (3 to 4 mm in length) in the right hemisphere region located 2 mm from the sagittal suture and 4 mm from the olfactory lobe, followed by an insertion with a 3 mm wide scalpel 2 mm deep into the cortex, controlled by a stereotactic arm. After injury the skin was sutured and animals received a subcutaneous buprenorphine injection (0.05 mg/kg body weight). Mice were kept and monitored for three days and then

anaesthetized (see above) and sacrificed by perfusion with 4% paraformaldehyde (PFA). Brains were incubated overnight in 4% PFA, washed with PBS, trimmed with a scalpel and mounted caudal side-down on a vibratome (Microm HM 650V, Thermo Scientific) stage using tissue glue (Loctite Super Glue). 35 μm thick coronal sections were made in the wound region and four representative sections were taken from each brain for immunostaining. Slices were permeabilized in 3% (v/v) TritonX (Roth) / 5% (v/v) donkey serum in PBS and incubated with anti-GFAP antibody (from rabbit, 1:1000, DAKO). Donkey anti-rabbit Alexa 555 antibody (1:1000, Invitrogen) was used to visualize the primary anti-GFAP antibody and nuclei were stained with DAPI. Slices were mounted on glass slides with mounting medium (Immu-Mount, Thermo Scientific) and pictures were taken as mosaic images with 10% overlap using a fluorescence microscope (Axiovert 200M, Zeiss) equipped with a 20x Plan-Apochromat (Zeiss) and a color camera (AxioCam, Zeiss), using the AxioVision Rel. 4.7 software. Images were analyzed with AxioVision by measuring three parameters: the area of reactive astrocytes (GFAP-stained cells), cortex edema as the increase in cortex thickness, and distribution of reactive astrocytes measured from the fluorescence intensity of the GFAP staining in defined squares along the cortex normalized to the mean fluorescence in the non-injured side (see Figure 7E).

Statistical Analysis

Data were analyzed using TILLvisION (Till Photonics), PatchMaster or Fitmaster (HEKA), Microsoft Excel, Igor Pro 5.1 (WaveMetrics), AxioVision Rel. 4.7 (Zeiss) and ImageJ (NIH). Data are shown as mean ± SEM with n indicating the number of patch-clamped cells, cells measured from × Ca^{2+} imaging experiments (n/x), scratches (migration) or wells (proliferation) measured in × independent cultures (n/x), or brain slices analyzed from × mice (n/x). To estimate the significance of differences, Student's t-test for two groups and one-way ANOVA followed by Bonferroni test for more than two groups were performed. The differences were assigned as significant if the P-value was < 0.05 (*), <0.01 (**) or < 0.001 (***).

Results

TRPC transcript expression in cultured mouse cortical astrocytes

Astrocytes and microglia were sorted by FACS (Supplementary Figure 1) into PCR tubes from cortical cell cultures prepared from 0–3 days old mice two to three weeks after isolation. TRPC transcripts were amplified by RT-PCR using 100 GLAST-positive astrocytes and 50 CD11b-positive microglial cells per tube. Consistently, *Trpc3* expression was identified in thirteen independent reactions using astrocytes from five independent sortings; *Trpc1* and *Trpc2* were identified in 10 reactions, *Trpc4* in 11 of 13 reactions, whereas *Trpc5*, *Trpc6* and *Trpc7* were not detectable (Figure 1A). In contrast, microglial cells did express *Trpc4* in three PCRs from three independent sortings, whereas *Trpc1*, *Trpc3*, *Trpc5*, *Trpc6* and *Trpc7* were not detectable (Figure 1B). The clear difference between the *Trpc* expression profile from sorted astrocytes and microglial cells shows the accuracy of the sorting. All *Trpc* transcripts were detectable using mouse brain RNA (Figure 1C) as control. The expression of *Trpc3 and Trpc1* transcripts was confirmed by RNA sequencing (Supplementary Figure 2). Similar expression levels as for *Trpc3* and *Trpc1* were

identified for transcripts of NMDA receptors (*Grin1, Grin2d and Grin3a*), metabotropic glutamate receptors (*Grm5*) or IP_3 receptors (*Itpr1 and Itpr2*; Supplementary Figure 2), known to be important for astrocyte function. The TRPC3 and TRPC1 proteins are present in mouse cortex (Figure 1D, E) and ultimate proof of *Trpc3* and *Trpc1* expression in astrocytes was obtained by amplifying the full-length cDNAs from the sorted cells (Figure 1F, G).

OAG-mediated cytosolic Ca^{2+} signals in cortical astrocytes depend on TRPC3

To study whether TRPC3 and TRPC1 are involved in Ca^{2+} signaling we performed Ca^{2+} imaging experiments in cultured astrocytes from wild-type mice and mice lacking the *Trpc3* and *Trpc1* genes. Intracellular Ca^{2+} stores were depleted in the absence of extracellular Ca^{2+} by thapsigargin (TG) or cyclopiazonic acid (CPA) followed by addition of extracellular Ca^{2+}, but no significant contribution of TRPC3 (and TRPC6, Figure 2A) or TRPC1 (Figure 2B) was observed. TRPC3 has been shown to be activated by 1-oleoyl-2-acetyl-sn-glycerol (OAG) (Hofmann et al., 1999), an analogue of diacylglycerol (DAG). In the presence of external Ca^{2+} bath application of 100 μM OAG induced Ca^{2+} oscillations in astrocytes (Figure 3A), but not in microglial cells (Figure 3C). Some OAG-mediated Ca^{2+} oscillations occurred in the absence of extracellular Ca^{2+} (Figure 3B), indicating that Ca^{2+} release from intracellular stores in addition to Ca^{2+} influx is affected by OAG. To separate Ca^{2+} influx from Ca^{2+} release the intracellular Ca^{2+} stores were depleted by 10 μM CPA in the presence of extracellular Ca^{2+} and OAG was applied on top. As shown in Figure 3D 100 μM OAG still induced significant Ca^{2+} oscillations which under these conditions depend on Ca^{2+} influx. Among *Trpc3*$^{-/-}$ astrocytes, less cells responded to OAG and those cells which responded showed less peaks compared to wild-type cells (Figure 3E, G, H, I).

In some experiments we used astrocytes from *Trpc6*$^{-/-}$ and *Trpc3*$^{-/-}$/*Trpc6*$^{-/-}$ mice. Since *Trpc6* is not detectable in the astrocytes (Figure 1A and Supplementary Figure 2), astrocytes from *Trpc6*$^{-/-}$ mice showed a very similar response as wild-type astrocytes, whereas OAG-induced Ca^{2+} influx is not significantly different in cells from *Trpc3*$^{-/-}$/*Trpc6*$^{-/-}$ and *Trpc3*$^{-/-}$ mice (Figure 3G, H, I). In contrast, the numbers of OAG-responding cells and of Ca^{2+} peaks per responding cell were higher among *Trpc1*$^{-/-}$ astrocytes compared to wild-type astrocytes (Figure 3F, G, H, I). These data indicate, that the OAG-mediated Ca^{2+} oscillations in astrocytes depend on TRPC3-mediated Ca^{2+} influx. Compared to wild-type, *Trpc3*-deficiency reduced and *Trpc1*-deficiency increased Ca^{2+} influx.

Functional interaction of TRPC3 and TRPC1

In the absence of *Trpc1* TRPC3 activity is increased (Figure 3F, G, H, I) and the apparent interaction of TRPC3 and TRPC1 was confirmed by co-immunoprecipitation of TRPC1 and TRPC3 by antibodies for both proteins (Figure 4A). Next the conditions to record TRPC3 currents in HEK cells by whole-cell patch clamp were optimized and a maximal OAG-induced TRPC3 current amplitude was obtained in the absence of extra- and intracellular Ca^{2+} (Figure 4B, C). However, under this condition the success rate of measuring OAG-mediated currents in astrocytes isolated from wild-type mice was very low, and only two cells out of more than 200 revealed a TRPC3-like current (Supplementary Figure 3). The following patch clamp experiments were therefore performed in the absence of intra- and

extracellular Ca^{2+} in HEK-293 cells. The amplitude of OAG-mediated TRPC3 currents were significantly reduced after co-expression of *Trpc1* (Figure 4D, E, F). Non-transfected HEK cells (control) and HEK cells only expressing *Trpc1* did not reveal any current upon OAG application (Figure 4D, E, F).

Moonwalker mice (mwk) harbor the TRPC3 T635A gain-of-function mutation. In astrocytes isolated from heterozygous mwk mice we detected a significantly higher basal Ca^{2+} level in the presence of extracellular Ca^{2+} (Figure 5A, C) and a significantly higher Ca^{2+} influx upon addition of external Ca^{2+} (Figure 5B, C) compared to astrocytes isolated from wild-type littermates. These data confirm that Ca^{2+} influx in astrocytes depends on TRPC3. To study the interaction with TRPC1 we generated a tetracycline-inducible $TRPC3_{T635A}$ HEK cell line. The spontaneous currents recorded two hours after induction were significantly reduced in the presence of *Trpc1* (Figure 5D, E, F, G). Non-induced (control) cells did not reveal a spontaneous current (Figure 5D, E, F, G). The latter results from patch clamp experiments were confirmed by Fura-2 Ca^{2+} imaging. Here the Ca^{2+} influx upon addition of extracellular Ca^{2+} and the basal Ca^{2+} level in the presence of extracellular Ca^{2+} were significantly higher in induced $TRPC3_{T635A}$ cells compared to these cells co-expressing *Trpc1* or cells which were not induced (control) by tetracycline (Figure 5H, I).

TRPC3 and TRPC1 are involved in expansion and migration of astrocytes *in vitro*

As shown *in vivo*, astrocytes rather proliferate and grow towards a lesion than actively migrate into the injury site (Bardehle et al., 2013). However, after performing a scratch in a confluent astrocyte layer *in vitro* astrocytes recover the cell-free area by proliferation, growth and migration (Zhan et al., 2016). The TRPC3-induced Ca^{2+} signals might translate into changes in proliferation, growth and migration of astrocytes. Astrocytes isolated from *Trpc3*$^{-/-}$ mice proliferated significantly slower compared to their corresponding wild-type cells, whereas astrocytes from heterozygous mwk and *Trpc1*$^{-/-}$ mice revealed a similar proliferation rate as wild-type controls (Supplementary Figure 4A). Supplementary figure 5 shows that astrocytes expand, migrate and recover the cell-free area from the boundary of the scratch and isolated cells invading the cell-free area are primarily microglial cells. Astrocytes lacking *Trpc3* or both *Trpc3* and *Trpc6* recovered a cell-free scratch area significantly slower than their corresponding wild-type cells, whereas astrocytes lacking only *Trpc6* responded, as expected, like wild-type, and astrocytes from heterozygous mwk and *Trpc1*$^{-/-}$ mice filled the scratched area of the cell monolayer significantly faster than the corresponding wild-type cells (Figure 6A, B). Accordingly, expansion and migration of astrocytes *in vitro* depends on TRPC3 and TRPC1. To study the proliferative activity of wild-type and *Trpc3*$^{-/-}$ astrocytes after injury, we performed the scratch assay in the presence of 10% FCS and quantified the percentage of proliferating cells using the proliferation marker anti-Ki-67. 24 hours after performing the scratch wild-type astrocytes revealed a significantly higher percentage of Ki-67-positive cells compared to *Trpc3*$^{-/-}$ astrocytes (Supplementary Figure 4B, C).

TRPC3 promotes astrogliosis and cortical edema in mice after cortical stab wound injury

To monitor astrogliosis as a measure of astrocyte function *in vivo*, defined cortical stab wounds were applied to *Trpc3*$^{-/-}$ and wild-type mice. Three days after lesion, the injured

areas were analyzed by fluorescence microscopy (see Figure 7A and E). The level of astrocyte activation was determined by immunostaining for GFAP (Figure 7A, C, E, F). Cortical edema were quantified in respect to the contralateral side of the injury (Figure 7A, E, G). To measure the distribution of GFAP-positive staining we defined squares along the cortex, determined the fluorescence intensity and normalized it to the fluorescence intensity of the non-injured hemisphere (Figure 7C, D, E). Brain slices from mice lacking *Trpc3* revealed significantly less edema and less GFAP-staining, i.e. less astrogliosis compared to wild-type mice (Figure 7A, C, F, G). To prove the results from GFAP staining, we quantified the amount of GFAP protein in injured hemispheres from the brain slices of wild-type and *Trpc3*$^{-/-}$ mice by western blot analysis: the injured hemisphere in *Trpc3*$^{-/-}$ mice revealed significantly less GFAP protein as compared to wild-type mice (Figure 7H, I). As already observed for the OAG-mediated cytosolic Ca^{2+} oscillations in isolated astrocytes (Figure 3) and *in vitro* migration experiments (Figure 6), the lack of *Trpc1* resulted in the opposite effects as the lack of *Trpc3*: The area of reactive astrocytes (Figure 7B, D, F) and of the cortical edema (Figure B, G) are significantly increased in mice lacking *Trpc1* compared to the corresponding wild-type mice.

Discussion

Upon brain injury, signaling molecules stimulate astrocyte proliferation, growth and their recruitment to the injured tissue (Burda & Sofroniew, 2014). These processes significantly depend on changes of the intracellular Ca^{2+} concentration (Gao et al., 2013; Kanemaru et al., 2013). In astrocytes signaling molecules as diverse as ATP, glutamate, thrombin and endothelin stimulate phospholipase C-coupled pathways resulting in IP_3-mediated Ca^{2+} release and mobilization of DAG. Among the cellular targets of DAG and its analogue OAG is the Ca^{2+}-permeable TRPC3 channel. In this study we show that OAG-induced Ca^{2+} oscillations depend on the presence of TRPC3 in cultured astrocytes, that TRPC3 promotes astrogliosis and cortical edema *in vivo*, and these TRPC3 activities are attenuated by TRPC1, both *in vitro* and *in vivo*.

TRPC3 and TRPC1 have been suggested to be present in diverse astrocytes and astrocytoma cells. OAG- and thrombin-mediated Ca^{2+} oscillations as well as ATP-, substance P- and bradykinin-induced Ca^{2+} signals in cultured rat cortical and spinal cord astrocytes, in 1321N1 human astrocytoma cells and in primary mouse striatal and cultured cortical astrocytes were suggested to depend on TRPCs (Akita & Okada, 2011; Grimaldi et al., 2003; Miyano et al., 2010; Nakao et al., 2008; Shirakawa et al., 2010; Streifel et al., 2014; Streifel et al., 2013) which presumably are involved in Na^+ and Ca^{2+} influx including store-operated Ca^{2+} entry in these cells (Golovina, 2005; Pizzo, Burgo, Pozzan, & Fasolato, 2001; Reyes et al., 2013). Using the appropriate *Trpc*-deficient mice as controls we could show that neither TRPC3 nor TRPC1 significantly contribute to Ca^{2+} entry after store-depletion in cultured cortical astrocytes (Figure 2).

The sparse data on TRPC3 function in astrocytes (see above) essentially rely on the use of the compound Pyrazolium 3 (Pyr3), which was first published as a specific TRPC3 antagonist (Kiyonaka et al., 2009). Munakata and colleagues (Munakata et al., 2013) showed that Pyr3 significantly reduced astrogliosis and brain edema in a mouse model of

intracerebral hemorrhage and they concluded that this effect was mediated by blocking TRPC3 function. Meanwhile, it has been shown that Pyr3 inhibits store-operated Orai1 channels with a similar potency as TRPC3 (Schleifer et al., 2012). Considering the expression levels of *orai1*, *stim1* and *stim2* in astrocytes (Supplementary Figure 2) the effects of Pyr3 on astrogliosis upon intracerebral hemorrhage might have been mediated by Orai/STIM channels.

Whereas Peters et al. (Peters et al., 2012) observed no significant change in the spontaneous recovery after closed head injury in *Trpc1*- or *Trpc3*-deficient mice compared with wild-type mice, Shirakawa et al. (Shirakawa et al., 2010) described a contribution of TRPC3 to pathological activation of astrocytes after intracortical injection of thrombin, and Nakao et al. (Nakao et al., 2008) suggested that thrombin-induced Ca^{2+} oscillations in 1321N1 human astrocytoma cells depend on Ca^{2+} release from intracellular stores, and that Ca^{2+} influx via TRPC3, itself not visible, refills the stores to sustain the oscillatory activity. However, in the present study the OAG-mediated TRPC3-dependent Ca^{2+} oscillations occur although the intracellular Ca^{2+} stores remain depleted by the continuous presence of CPA. These OAG-induced Ca^{2+} oscillations are increased in the absence of TRPC1.

TRPC1 and TRPC3 may form heterotetrameric TRPC1/TRPC3 channels (Cheung et al., 2011; Lintschinger et al., 2000; Liu, Bandyopadhyay, Singh, Groschner, & Ambudkar, 2005; Schaefer, 2005; Storch, Forst, Philipp, Gudermann, & Mederos y Schnitzler, 2012; Wang, Wang, & Li, 2016; Woo, Lee, Huang, Cho, & Lee, 2014; Wu, Zagranichnaya, Gurda, Eves, & Villereal, 2004). Heterotetrameric TRPC1/TRPC4 and TRPC1/TRPC5 channels reveal altered current-voltage relations and cation selectivity compared to homomeric TRPC4 and TRPC5 channels (Storch et al., 2012; Strubing, Krapivinsky, Krapivinsky, & Clapham, 2001), but although TRPC1/TRPC3 currents had reduced current amplitudes compared to TRPC3 currents their current-voltage relations and cation selectivity were apparently not different (Figure 4). So far, we did not address the mechanism of TRPC1-dependent inhibition of TRPC3 in astrocytes, but TRPC1 might be an inhibitory ion conducting subunit of heterotetrameric TRPC1/TRPC3 channels, act as an auxiliary inhibitory and non-conducting beta subunit for TRPC3 channels or inhibit the plasma membrane targeting of TRPC3. TRPC1 does significantly mitigate constitutive mwk-induced Ca^{2+} entry; apparently it does not discriminate between wild-type TRPC3 and its gain-of-function moonwalker mutation.

Our observation that lack of *Trpc3* reduced astrocyte proliferation and migration, whereas the TRPC3 moonwalker mutant and the lack of *Trpc1* increased migration are compatible with TRPC3 activity promoting proliferation and migration of cortical astrocytes. Table 2 lists several genes which are involved in proliferation and migration in diverse other cell types and which are significantly downregulated in *Trpc3*-deficient astrocytes compared with the same genes in astrocytes from wild-type mice. The microarray analysis on independent mRNA extracted from sorted wild-type and *Trpc3*-deficient astrocytes was performed in biological triplicates and revealed no significant change of expression of other *Trpc* genes or genes of other Ca^{2+}-permeable ion channels.

Astrocytes in culture mostly reveal a prominent expression of GFAP (see e.g. Supplement Figure 1A), whereas astrocytes in the intact brain usually exhibit low GFAP expression (see e.g. Figure 7A - non-injured hemispheres). Thus, astrocytes *in vitro* seem to be in a more reactive state compared to astrocytes *in vivo*, i.e. conditions *in vitro* and *in vivo* might be different. In addition, properties and functions of astrocytes in different brain areas and at different ages are also versatile. However, our data on cultured cells isolated from the cortex of newborn mice and the stab wound data on adult mice both suggest significant functions of TRPC3 and TRPC1 in the cortical astrocytes.

In summary, TRPC3-induced Ca^{2+} entry promotes astrocyte proliferation and migration i.e. astrocyte activity *in vitro* which is attenuated by the presence of TRPC1. Following brain injury, the absence of TRPC3 results in a significant reduction of astrogliosis and cortical edema *in vivo*, suggesting that a targeted therapy to reduce TRPC3 channel activity, for example by increasing formation of heteromeric TRPC3/TRPC1 channels, might be beneficial in traumatic brain injury.

Supplementary Material

Refer to Web version on PubMed Central for supplementary material.

Acknowledgments

We thank the members of the Homburg SPF-animal facility and Stefanie Buchholz, Christine Wesely, Heidi Löhr, Sandra Plant, Carsten Schröder and Martin Simon-Thomas for expert technical assistance, and Luam Araya for proofreading the manuscript as native speaker. This work was supported by the Deutsche Forschungsgemeinschaft (GRK1326, T.B., A.B.; IRTG1830, L.H., V.F.; SFB894, A.B., V.F., P.W., S.E.P., F.K.), the Homburg Forschungsförderungsprogramm HOMFOR (A.B., A.S., S.E.P.), the Forschungskommission der Universität des Saarlandes (A.B., P.W., S.E.P., V.F.), and the Intramural Research Program of the NIH Project ZO1-ES101684 (L.B.).

References

Ait-Lounis A, Bonal C, Seguin-Estevez Q, Schmid CD, Bucher P, Herrera PL, Reith W. The transcription factor Rfx3 regulates beta-cell differentiation, function, and glucokinase expression. Diabetes. 2010; 59(7):1674–1685. DOI: 10.2337/db09-0986 [PubMed: 20413507]

Akita T, Okada Y. Regulation of bradykinin-induced activation of volume-sensitive outwardly rectifying anion channels by Ca2+ nanodomains in mouse astrocytes. J Physiol. 2011; 589(Pt 16): 3909–3927. DOI: 10.1113/jphysiol.2011.208173 [PubMed: 21690189]

Bardehle S, Kruger M, Buggenthin F, Schwausch J, Ninkovic J, Clevers H, Gotz M. Live imaging of astrocyte responses to acute injury reveals selective juxtavascular proliferation. Nat Neurosci. 2013; 16(5):580–586. DOI: 10.1038/nn.3371 [PubMed: 23542688]

Beck A, Speicher T, Stoerger C, Sell T, Dettmer V, Jusoh SA, Flockerzi V. Conserved gating elements in TRPC4 and TRPC5 channels. J Biol Chem. 2013; 288(27):19471–19483. DOI: 10.1074/jbc.M113.478305 [PubMed: 23677990]

Becker EB. The Moonwalker mouse: new insights into TRPC3 function, cerebellar development, and ataxia. Cerebellum. 2014; 13(5):628–636. DOI: 10.1007/s12311-014-0564-5 [PubMed: 24797279]

Becker EB, Oliver PL, Glitsch MD, Banks GT, Achilli F, Hardy A, Davies KE. A point mutation in TRPC3 causes abnormal Purkinje cell development and cerebellar ataxia in moonwalker mice. Proc Natl Acad Sci U S A. 2009; 106(16):6706–6711. DOI: 10.1073/pnas.0810599106 [PubMed: 19351902]

Beskina O, Miller A, Mazzocco-Spezzia A, Pulina MV, Golovina VA. Mechanisms of interleukin-1beta-induced Ca2+ signals in mouse cortical astrocytes: roles of store- and receptor-

operated Ca2+ entry. Am J Physiol Cell Physiol. 2007; 293(3):C1103–1111. DOI: 10.1152/ajpcell.00249.2007 [PubMed: 17670890]

Bhattaram P, Penzo-Mendez A, Sock E, Colmenares C, Kaneko KJ, Vassilev A, Lefebvre V. Organogenesis relies on SoxC transcription factors for the survival of neural and mesenchymal progenitors. Nat Commun. 2010; 1:9.doi: 10.1038/ncomms1008 [PubMed: 20596238]

Bomben VC, Sontheimer H. Disruption of transient receptor potential canonical channel 1 causes incomplete cytokinesis and slows the growth of human malignant gliomas. Glia. 2010; 58(10): 1145–1156. DOI: 10.1002/glia.20994 [PubMed: 20544850]

Bomben VC, Turner KL, Barclay TT, Sontheimer H. Transient receptor potential canonical channels are essential for chemotactic migration of human malignant gliomas. J Cell Physiol. 2011; 226(7): 1879–1888. DOI: 10.1002/jcp.22518 [PubMed: 21506118]

Burda JE, Sofroniew MV. Reactive gliosis and the multicellular response to CNS damage and disease. Neuron. 2014; 81(2):229–248. DOI: 10.1016/j.neuron.2013.12.034 [PubMed: 24462092]

Cheung KK, Yeung SS, Au SW, Lam LS, Dai ZQ, Li YH, Yeung EW. Expression and association of TRPC1 with TRPC3 during skeletal myogenesis. Muscle Nerve. 2011; 44(3):358–365. DOI: 10.1002/mus.22060 [PubMed: 21996795]

Chun C, Wu Y, Lee SH, Williamson EA, Reinert BL, Jaiswal AS, Hromas RA. The homologous recombination component EEPD1 is required for genome stability in response to developmental stress of vertebrate embryogenesis. Cell Cycle. 2016; 15(7):957–962. DOI: 10.1080/15384101.2016.1151585 [PubMed: 26900729]

Deliot N, Constantin B. Plasma membrane calcium channels in cancer: Alterations and consequences for cell proliferation and migration. Biochim Biophys Acta. 2015; 1848(10 Pt B):2512–2522. DOI: 10.1016/j.bbamem.2015.06.009 [PubMed: 26072287]

Dietrich A, Kalwa H, Storch U, Mederos y Schnitzler M, Salanova B, Pinkenburg O, Gudermann T. Pressure-induced and store-operated cation influx in vascular smooth muscle cells is independent of TRPC1. Pflugers Arch. 2007; 455(3):465–477. DOI: 10.1007/s00424-007-0314-3 [PubMed: 17647013]

Duong Van Huyen JP, Cheval L, Bloch-Faure M, Belair MF, Heudes D, Bruneval P, Doucet A. GDF15 triggers homeostatic proliferation of acid-secreting collecting duct cells. J Am Soc Nephrol. 2008; 19(10):1965–1974. DOI: 10.1681/ASN.2007070781 [PubMed: 18650486]

Dutton RP, McCunn M. Traumatic brain injury. Curr Opin Crit Care. 2003; 9(6):503–509. [PubMed: 14639070]

Faul M, Xu L, Wald MM, Coronado V, Dellinger AM. Traumatic Brain Injury in the United States: National Estimates of Prevalence and Incidence, 2002–2006. Injury Prevention. 2010; 16:A268–A268. DOI: 10.1136/ip.2010.029951

Gao K, Wang CR, Jiang F, Wong AY, Su N, Jiang JH, Yu AC. Traumatic scratch injury in astrocytes triggers calcium influx to activate the JNK/c-Jun/AP-1 pathway and switch on GFAP expression. Glia. 2013; 61(12):2063–2077. DOI: 10.1002/glia.22577 [PubMed: 24123203]

Gatza ML, Silva GO, Parker JS, Fan C, Perou CM. An integrated genomics approach identifies drivers of proliferation in luminal-subtype human breast cancer. Nat Genet. 2014; 46(10):1051–1059. DOI: 10.1038/ng.3073 [PubMed: 25151356]

Golovina VA. Visualization of localized store-operated calcium entry in mouse astrocytes. Close proximity to the endoplasmic reticulum. J Physiol. 2005; 564(Pt 3):737–749. DOI: 10.1113/jphysiol.2005.085035 [PubMed: 15731184]

Grimaldi M, Maratos M, Verma A. Transient receptor potential channel activation causes a novel form of [Ca 2+]I oscillations and is not involved in capacitative Ca 2+ entry in glial cells. J Neurosci. 2003; 23(11):4737–4745. [PubMed: 12805313]

Hartmann J, Dragicevic E, Adelsberger H, Henning HA, Sumser M, Abramowitz J, Konnerth A. TRPC3 channels are required for synaptic transmission and motor coordination. Neuron. 2008; 59(3):392–398. DOI: 10.1016/j.neuron.2008.06.009 [PubMed: 18701065]

Hofmann T, Obukhov AG, Schaefer M, Harteneck C, Gudermann T, Schultz G. Direct activation of human TRPC6 and TRPC3 channels by diacylglycerol. Nature. 1999; 397(6716):259–263. DOI: 10.1038/16711 [PubMed: 9930701]

Kanemaru K, Kubota J, Sekiya H, Hirose K, Okubo Y, Iino M. Calcium-dependent N-cadherin up-regulation mediates reactive astrogliosis and neuroprotection after brain injury. Proc Natl Acad Sci U S A. 2013; 110(28):11612–11617. DOI: 10.1073/pnas.1300378110 [PubMed: 23798419]

Kiyonaka S, Kato K, Nishida M, Mio K, Numaga T, Sawaguchi Y, Mori Y. Selective and direct inhibition of TRPC3 channels underlies biological activities of a pyrazole compound. Proc Natl Acad Sci U S A. 2009; 106(13):5400–5405. DOI: 10.1073/pnas.0808793106 [PubMed: 19289841]

Kuang CY, Yu Y, Wang K, Qian DH, Den MY, Huang L. Knockdown of transient receptor potential canonical-1 reduces the proliferation and migration of endothelial progenitor cells. Stem Cells Dev. 2012; 21(3):487–496. DOI: 10.1089/scd.2011.0027 [PubMed: 21361857]

Kwiatkowski AV, Gertler FB, Loureiro JJ. Function and regulation of Ena/VASP proteins. Trends Cell Biol. 2003; 13(7):386–392. [PubMed: 12837609]

Lee MP, Yutzey KE. Twist1 directly regulates genes that promote cell proliferation and migration in developing heart valves. PLoS One. 2011; 6(12):e29758.doi: 10.1371/journal.pone.0029758 [PubMed: 22242143]

Li B, Dong L, Fu H, Wang B, Hertz L, Peng L. Effects of chronic treatment with fluoxetine on receptor-stimulated increase of [Ca2+]i in astrocytes mimic those of acute inhibition of TRPC1 channel activity. Cell Calcium. 2011; 50(1):42–53. DOI: 10.1016/j.ceca.2011.05.001 [PubMed: 21640379]

Lintschinger B, Balzer-Geldsetzer M, Baskaran T, Graier WF, Romanin C, Zhu MX, Groschner K. Coassembly of Trp1 and Trp3 proteins generates diacylglycerol- and Ca2+-sensitive cation channels. J Biol Chem. 2000; 275(36):27799–27805. DOI: 10.1074/jbc.M002705200 [PubMed: 10882720]

Liu X, Bandyopadhyay BC, Singh BB, Groschner K, Ambudkar IS. Molecular analysis of a store-operated and 2-acetyl-sn-glycerol-sensitive non-selective cation channel. Heteromeric assembly of TRPC1-TRPC3. J Biol Chem. 2005; 280(22):21600–21606. DOI: 10.1074/jbc.C400492200 [PubMed: 15834157]

Loikkanen I, Lin Y, Railo A, Pajunen A, Vainio S. Polyamines are involved in murine kidney development controlling expression of c-ret, E-cadherin, and Pax2/8 genes. Differentiation. 2005; 73(6):303–312. DOI: 10.1111/j.1432-0436.2005.00036.x [PubMed: 16138831]

Malarkey EB, Ni Y, Parpura V. Ca2+ entry through TRPC1 channels contributes to intracellular Ca2+ dynamics and consequent glutamate release from rat astrocytes. Glia. 2008; 56(8):821–835. DOI: 10.1002/glia.20656 [PubMed: 18338793]

Miyano K, Morioka N, Sugimoto T, Shiraishi S, Uezono Y, Nakata Y. Activation of the neurokinin-1 receptor in rat spinal astrocytes induces Ca2+ release from IP3-sensitive Ca2+ stores and extracellular Ca2+ influx through TRPC3. Neurochem Int. 2010; 57(8):923–934. DOI: 10.1016/j.neuint.2010.09.012 [PubMed: 20933035]

Munakata M, Shirakawa H, Nagayasu K, Miyanohara J, Miyake T, Nakagawa T, Kaneko S. Transient receptor potential canonical 3 inhibitor Pyr3 improves outcomes and attenuates astrogliosis after intracerebral hemorrhage in mice. Stroke. 2013; 44(7):1981–1987. DOI: 10.1161/STROKEAHA.113.679332 [PubMed: 23674527]

Nakao K, Shirakawa H, Sugishita A, Matsutani I, Niidome T, Nakagawa T, Kaneko S. Ca2+ mobilization mediated by transient receptor potential canonical 3 is associated with thrombin-induced morphological changes in 1321N1 human astrocytoma cells. J Neurosci Res. 2008; 86(12):2722–2732. DOI: 10.1002/jnr.21711 [PubMed: 18478545]

Peters M, Trembovler V, Alexandrovich A, Parnas M, Birnbaumer L, Minke B, Shohami E. Carvacrol together with TRPC1 elimination improve functional recovery after traumatic brain injury in mice. J Neurotrauma. 2012; 29(18):2831–2834. DOI: 10.1089/neu.2012.2575 [PubMed: 22994850]

Pizzo P, Burgo A, Pozzan T, Fasolato C. Role of capacitative calcium entry on glutamate-induced calcium influx in type-I rat cortical astrocytes. J Neurochem. 2001; 79(1):98–109. [PubMed: 11595762]

Quick K, Zhao J, Eijkelkamp N, Linley JE, Rugiero F, Cox JJ, Wood JN. TRPC3 and TRPC6 are essential for normal mechanotransduction in subsets of sensory neurons and cochlear hair cells. Open Biol. 2012; 2(5):120068.doi: 10.1098/rsob.120068 [PubMed: 22724068]

Reyes RC, Verkhratsky A, Parpura V. TRPC1-mediated Ca2+ and Na+ signalling in astroglia: differential filtering of extracellular cations. Cell Calcium. 2013; 54(2):120–125. DOI: 10.1016/j.ceca.2013.05.005 [PubMed: 23764169]

Schaefer M. Homo- and heteromeric assembly of TRP channel subunits. Pflugers Arch. 2005; 451(1): 35–42. DOI: 10.1007/s00424-005-1467-6 [PubMed: 15971080]

Schleifer H, Doleschal B, Lichtenegger M, Oppenrieder R, Derler I, Frischauf I, Groschner K. Novel pyrazole compounds for pharmacological discrimination between receptor-operated and store-operated Ca(2+) entry pathways. Br J Pharmacol. 2012; 167(8):1712–1722. DOI: 10.1111/j.1476-5381.2012.02126.x [PubMed: 22862290]

Shirakawa H, Sakimoto S, Nakao K, Sugishita A, Konno M, Iida S, Kaneko S. Transient receptor potential canonical 3 (TRPC3) mediates thrombin-induced astrocyte activation and upregulates its own expression in cortical astrocytes. J Neurosci. 2010; 30(39):13116–13129. DOI: 10.1523/JNEUROSCI.1890-10.2010 [PubMed: 20881130]

Sofroniew MV. Molecular dissection of reactive astrogliosis and glial scar formation. Trends Neurosci. 2009; 32(12):638–647. DOI: 10.1016/j.tins.2009.08.002 [PubMed: 19782411]

Song X, Zhao Y, Narcisse L, Duffy H, Kress Y, Lee S, Brosnan CF. Canonical transient receptor potential channel 4 (TRPC4) co-localizes with the scaffolding protein ZO-1 in human fetal astrocytes in culture. Glia. 2005; 49(3):418–429. DOI: 10.1002/glia.20128 [PubMed: 15540229]

Storch U, Forst AL, Philipp M, Gudermann T, Mederos y Schnitzler M. Transient receptor potential channel 1 (TRPC1) reduces calcium permeability in heteromeric channel complexes. J Biol Chem. 2012; 287(5):3530–3540. DOI: 10.1074/jbc.M111.283218 [PubMed: 22157757]

Streifel KM, Gonzales AL, De Miranda B, Mouneimne R, Earley S, Tjalkens R. Dopaminergic neurotoxicants cause biphasic inhibition of purinergic calcium signaling in astrocytes. PLoS One. 2014; 9(11):e110996.doi: 10.1371/journal.pone.0110996 [PubMed: 25365260]

Streifel KM, Miller J, Mouneimne R, Tjalkens RB. Manganese inhibits ATP-induced calcium entry through the transient receptor potential channel TRPC3 in astrocytes. Neurotoxicology. 2013; 34:160–166. DOI: 10.1016/j.neuro.2012.10.014 [PubMed: 23131343]

Strubing C, Krapivinsky G, Krapivinsky L, Clapham DE. TRPC1 and TRPC5 form a novel cation channel in mammalian brain. Neuron. 2001; 29(3):645–655. [PubMed: 11301024]

Tagliaferri F, Compagnone C, Korsic M, Servadei F, Kraus J. A systematic review of brain injury epidemiology in Europe. Acta Neurochirurgica. 2006; 148(3):255–268. DOI: 10.1007/s00701-005-0651-y [PubMed: 16311842]

Trapnell C, Pachter L, Salzberg SL. TopHat: discovering splice junctions with RNA-Seq. Bioinformatics. 2009; 25(9):1105–1111. DOI: 10.1093/bioinformatics/btp120 [PubMed: 19289445]

Trapnell C, Roberts A, Goff L, Pertea G, Kim D, Kelley DR, Pachter L. Differential gene and transcript expression analysis of RNA-seq experiments with TopHat and Cufflinks. Nat Protoc. 2012; 7(3):562–578. DOI: 10.1038/nprot.2012.016 [PubMed: 22383036]

Tsvilovskyy VV, Zholos AV, Aberle T, Philipp SE, Dietrich A, Zhu MX, Flockerzi V. Deletion of TRPC4 and TRPC6 in mice impairs smooth muscle contraction and intestinal motility in vivo. Gastroenterology. 2009; 137(4):1415–1424. DOI: 10.1053/j.gastro.2009.06.046 [PubMed: 19549525]

Wang Y, Wang Y, Li GR. TRPC1/TRPC3 channels mediate lysophosphatidylcholine-induced apoptosis in cultured human coronary artery smooth muscles cells. Oncotarget. 2016; doi: 10.18632/oncotarget.10853

Windle WF, Clemente CD, Chambers WW. Inhibition of formation of a glial barrier as a means of permitting a peripheral nerve to grow into the brain. J Comp Neurol. 1952; 96(2):359–369. [PubMed: 14938473]

Woo JS, Lee KJ, Huang M, Cho CH, Lee EH. Heteromeric TRPC3 with TRPC1 formed via its ankyrin repeats regulates the resting cytosolic Ca2+ levels in skeletal muscle. Biochem Biophys Res Commun. 2014; 446(2):454–459. DOI: 10.1016/j.bbrc.2014.02.127 [PubMed: 24613381]

Wu X, Zagranichnaya TK, Gurda GT, Eves EM, Villereal ML. A TRPC1/TRPC3-mediated increase in store-operated calcium entry is required for differentiation of H19-7 hippocampal neuronal cells. J Biol Chem. 2004; 279(42):43392–43402. DOI: 10.1074/jbc.M408959200 [PubMed: 15297455]

Zhan JS, Gao K, Chai RC, Jia XH, Luo DP, Ge G, Yu AC. Astrocytes in Migration. Neurochem Res. 2016; doi: 10.1007/s11064-016-2089-4

Zhao Z, Ni Y, Chen J, Zhong J, Yu H, Xu X, Tepel M. Increased migration of monocytes in essential hypertension is associated with increased transient receptor potential channel canonical type 3 channels. PLoS One. 2012; 7(3):e32628.doi: 10.1371/journal.pone.0032628 [PubMed: 22438881]

Zhu X, Jiang M, Birnbaumer L. Receptor-activated Ca2+ influx via human Trp3 stably expressed in human embryonic kidney (HEK)293 cells. Evidence for a non-capacitative Ca2+ entry. J Biol Chem. 1998; 273(1):133–142. [PubMed: 9417057]

Zimmermann J, Latta L, Beck A, Leidinger P, Fecher-Trost C, Schlenstedt G, Flockerzi V. Trans-activation response (TAR) RNA-binding protein 2 is a novel modulator of transient receptor potential canonical 4 (TRPC4) protein. J Biol Chem. 2014; 289(14):9766–9780. DOI: 10.1074/jbc.M114.557066 [PubMed: 24563462]

Main points

- Cortical astrocytes functionally express Ca^{2+}-permeable TRPC3 channels.
- TRPC3 promotes astrogliosis and cortical edema following a cortical stab wound injury.
- The decisive contribution of TRPC3 to astrocyte Ca^{2+} signaling is mitigated by TRPC1.

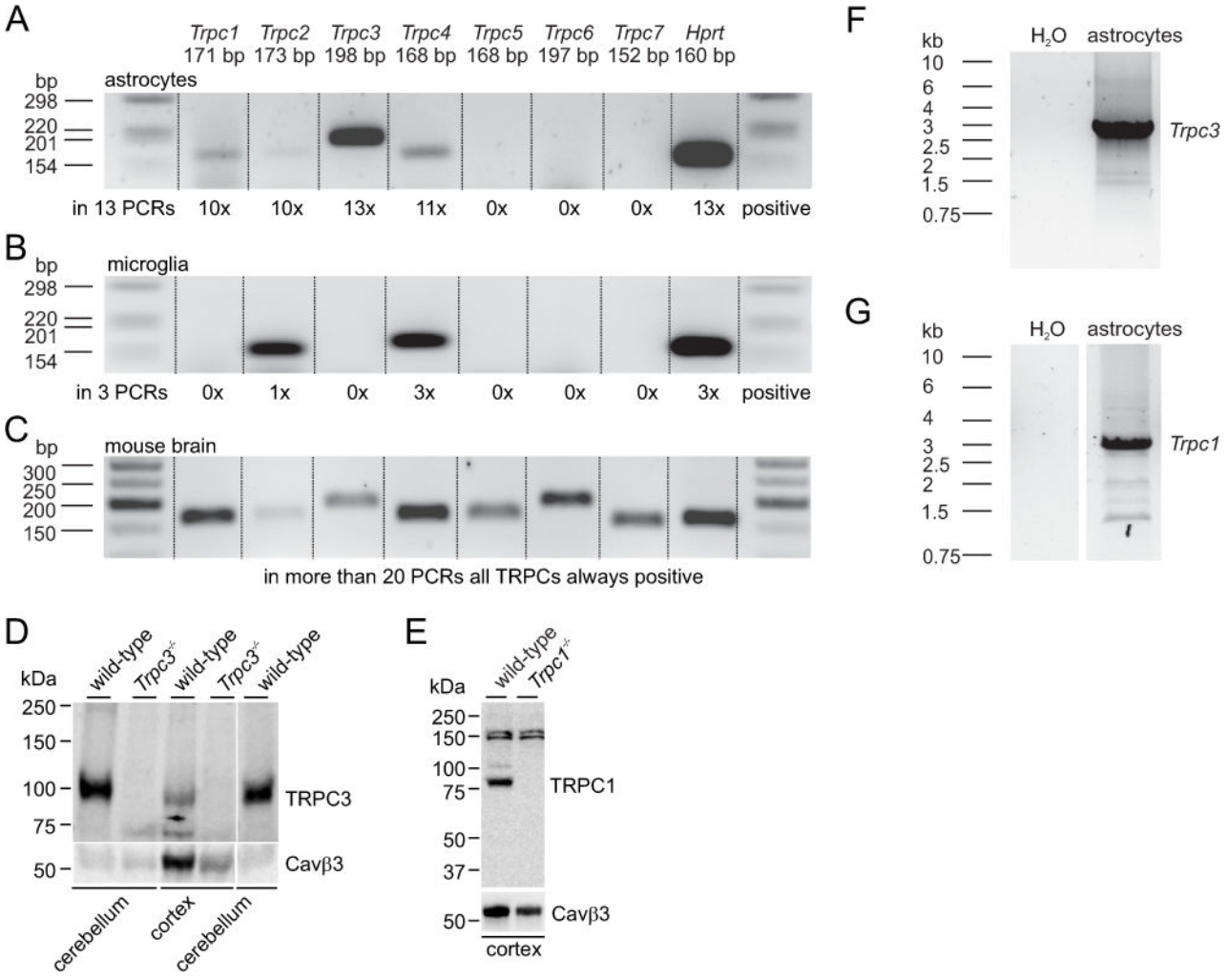

Figure 1. Cortical astrocytes express *Trpc3* and *Trpc1*

(**A**–**C**) RT-PCRs performed from 100 FACS-sorted GLAST-positive astrocytes (A), 50 FACS-sorted CD11b-positive microglial cells (B) and mouse brain RNA (C). The frequencies of amplified *Trpc* transcripts in astrocytes in 13 independent RT-PCRs from 5 independent sortings and in microglia in 3 independent RT-PCRs from 3 independent sortings are shown below the blots. *Hprt* served as positive control. First and last lanes in A, B and C show marker DNAs. (**D**, **E**) Immunoblot analysis of TRPC3 (D) and TRPC1 (E) proteins in lysates from mouse cerebellum and cortex (100 µg/lane) extracted from wild-type and *Trpc3*$^{-/-}$ mice or *Trpc1*$^{-/-}$ mice revealed the loss of TRPC3 and TRPC1 proteins in *Trpc3*$^{-/-}$ and *Trpc1*$^{-/-}$ mice, respectively. To confirm equal loading of samples independent blots running in parallel were probed with a Cavβ3 antibody. (**F**, **G**) Full-length amplification of *Trpc3* (F) and *Trpc1* (G) cDNAs from cultured cortical Glast-postive FACS-sorted astrocytes.

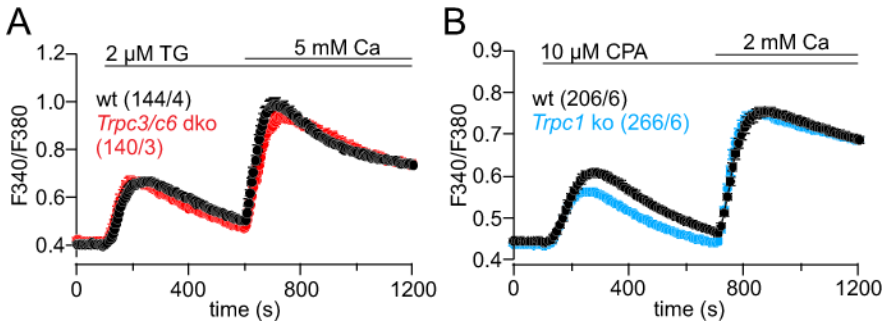

Figure 2. Ca^{2+} influx after store depletion does not depend on TRPC3, TRPC6 or TRPC1 in cortical astrocytes

(**A**, **B**) Ca^{2+} release induced by 2 µM thapsigargin (TG, A) or 10 µM cyclopiazonic acid (CPA, B) in the absence of extracellular Ca^{2+} and subsequent Ca^{2+} entry upon Ca^{2+} readdition in astrocytes from *Trpc3*$^{-/-}$/*Trpc6*$^{-/-}$ (*Trpc3/c6* dko, A) and *Trpc1*$^{-/-}$ mice (*Trpc1* ko, B) and their corresponding wild-types (wt), measured as Fura-2 ratio F340/F380. Data represent means ± S.E.M. of n cells from × experiments (n/x).

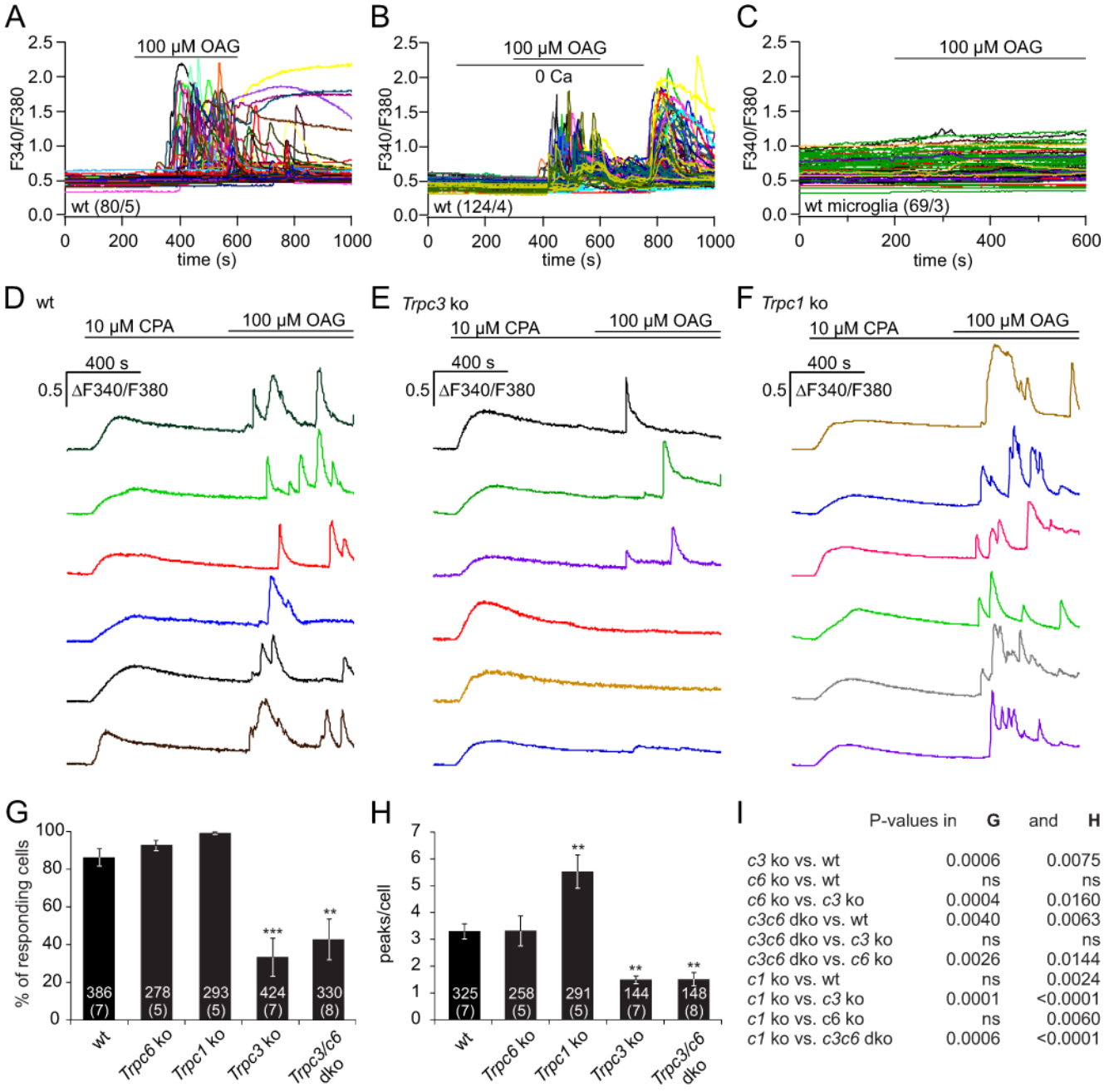

Figure 3. OAG-mediated Ca^{2+} influx depends on *Trpc3*.

(**A**, **B**) OAG-induced cytoplasmic Ca^{2+} increase in astrocytes in the presence (A) and absence of extracellular Ca^{2+} (B), and upon addition of Ca^{2+} to the bath as indicated (B). (**C**) Microglial cells do not reveal a change of cytoplasmic Ca^{2+} upon OAG application. (**D**–**F**) OAG-induced Ca^{2+} entry in the presence of extracellular Ca^{2+} (2 mM) at sustained store depletion by cyclopiazonic acid (CPA, 10 µM) present throughout the experiment in astrocytes from wild-type (wt, D), *Trpc3*$^{-/-}$ (*Trpc3* ko, E) and *Trpc1*$^{-/-}$ (*Trpc1* ko, F) mice. (**G**, **H**) Percentage of OAG-responding cells (G) and number of OAG-mediated Ca^{2+} peaks per responding cell (H) in astrocytes from wild-type, *Trpc6*$^{-/-}$, *Trpc1*$^{-/-}$, *Trpc3*$^{-/-}$ and

Trpc3$^{-/-}$/*c6*$^{-/-}$ mice. Data represent means ± S.E.M. (n, number of cells from x, number of experiments (n/x)) with asterisks in G and H marking significant differences compared to the wild-type (** P<0.01, *** P<0.001). (**I**) P-values for comparisons in G and H were obtained by one-way ANOVA followed by Bonferroni test.

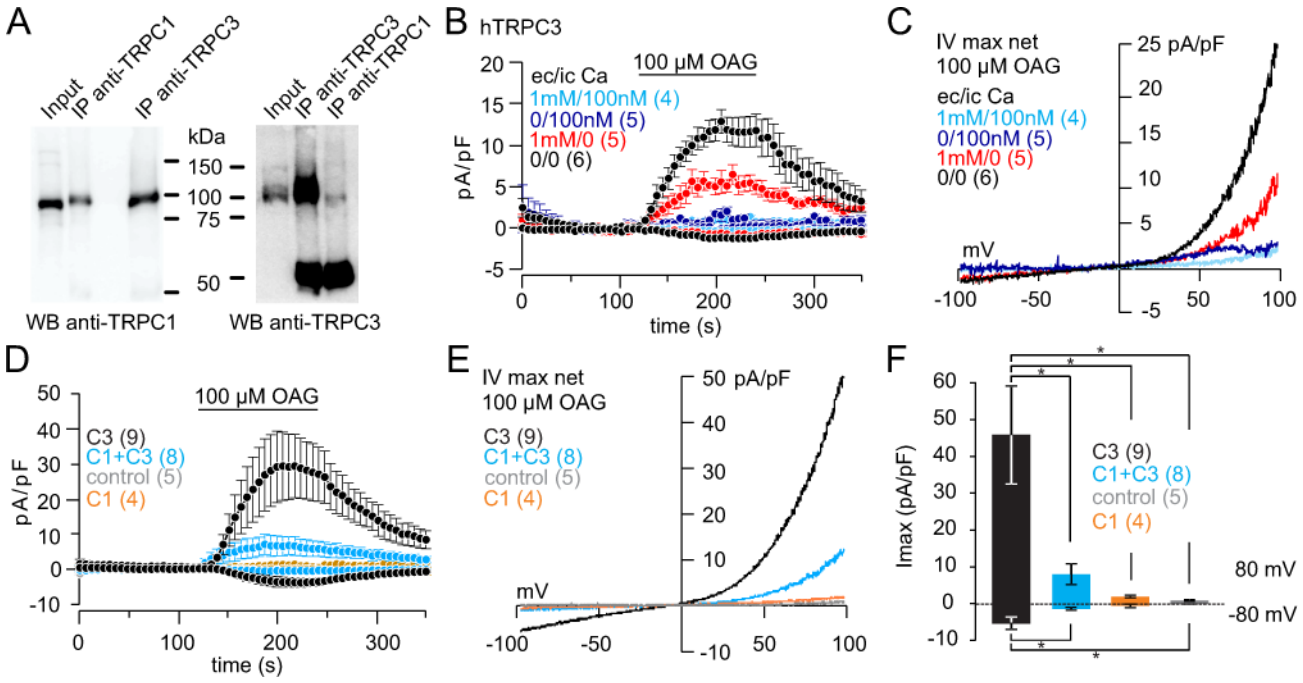

Figure 4. Interaction of TRPC3 and TRPC1

(**A**) Co-immunoprecipitation of TRPC3 and TRPC1 and *vice versa* from lysates of HEK cells transfected with the *Trpc1* and *Trpc3* cDNAs. (**B**) 100 µM OAG-induced TRPC3 inward and outward currents at −80 and +80 mV in the absence and presence of extracellular (ec) Ca^{2+} (1 mM) or intracellular (ic) Ca^{2+} (100 nM), in HEK cells stably expressing human (h) TRPC3. (**C**) Corresponding current-voltage relationships of currents in B. (**D**–**F**) OAG-induced inward and outward currents in HEK wild-type cells and HEK cells stably expressing *Trpc1* without (control and C1) and with transient expression of *Trpc3* cDNA (C3 and C1+C3). Current voltage relationships and differences (* $P<0.05$) of current amplitudes are shown in E and F, respectively. Inward and outward currents are means ± S.E.M. of n cells.

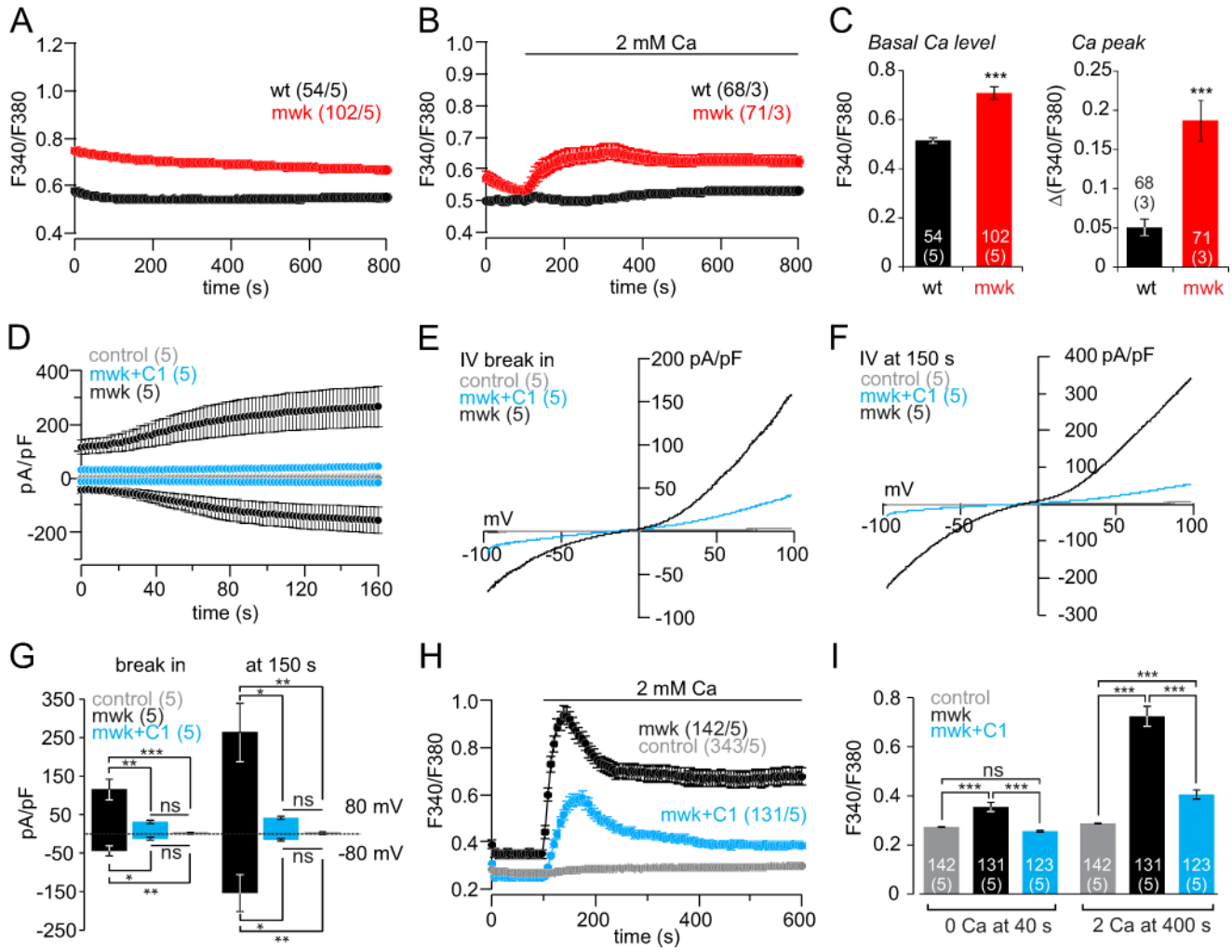

Figure 5. Constitutive activity of the TRPC3$_{T635A}$ moonwalker (mwk) mutant is antagonized by *Trpc1* expression

(**A**, **B**) Changes of cytoplasmic Ca^{2+} (F340/F380) in cultured cortical astrocytes isolated from wild-type (wt) and heterozygous TRPC3$_{T635A}$ moonwalker (mwk) mice in the presence (A), absence (B, 0–100 s) and after addition (B, application bar) of extracellular Ca^{2+}. (**C**) Basal cytoplasmic Ca^{2+} (F340/F380) in A and ΔF340/F380 upon Ca^{2+} readdition in B. (**D**–**G**) Spontaneous inward and outward currents at −80 mV and +80 mV in the tetracycline-inducible HEK TRPC3$_{T635A}$ (mwk) cell line. Control, no tetracycline induction; mwk, after tetracycline induction; mwk+C1, after tetracycline induction and transfection with the *Trpc1* cDNA. Current-voltage relationships at break in (E) and at 150 s (F) and corresponding current amplitudes at −80 mV and +80 mV (G), plotted as means ± S.E.M. (n, number of cells). (**H**, **I**) Basal cytoplasmic Ca^{2+} and increase of cytoplasmic Ca^{2+} upon addition of 2 mM extracellular Ca^{2+}. Control, no tetracycline induction; mwk, after tetracycline induction; mwk+C1, after tetracycline induction and transfection with the *Trpc1* cDNA. Cytoplasmic Ca^{2+} at 40 s and at 400 s (I) plotted as mean ± S.E.M. (n, number of cells from x, number of experiments (n/x)). Asterisks assign significant differences (* P<0.05, ** P<0.01, *** P<0.001, ns = not significant).

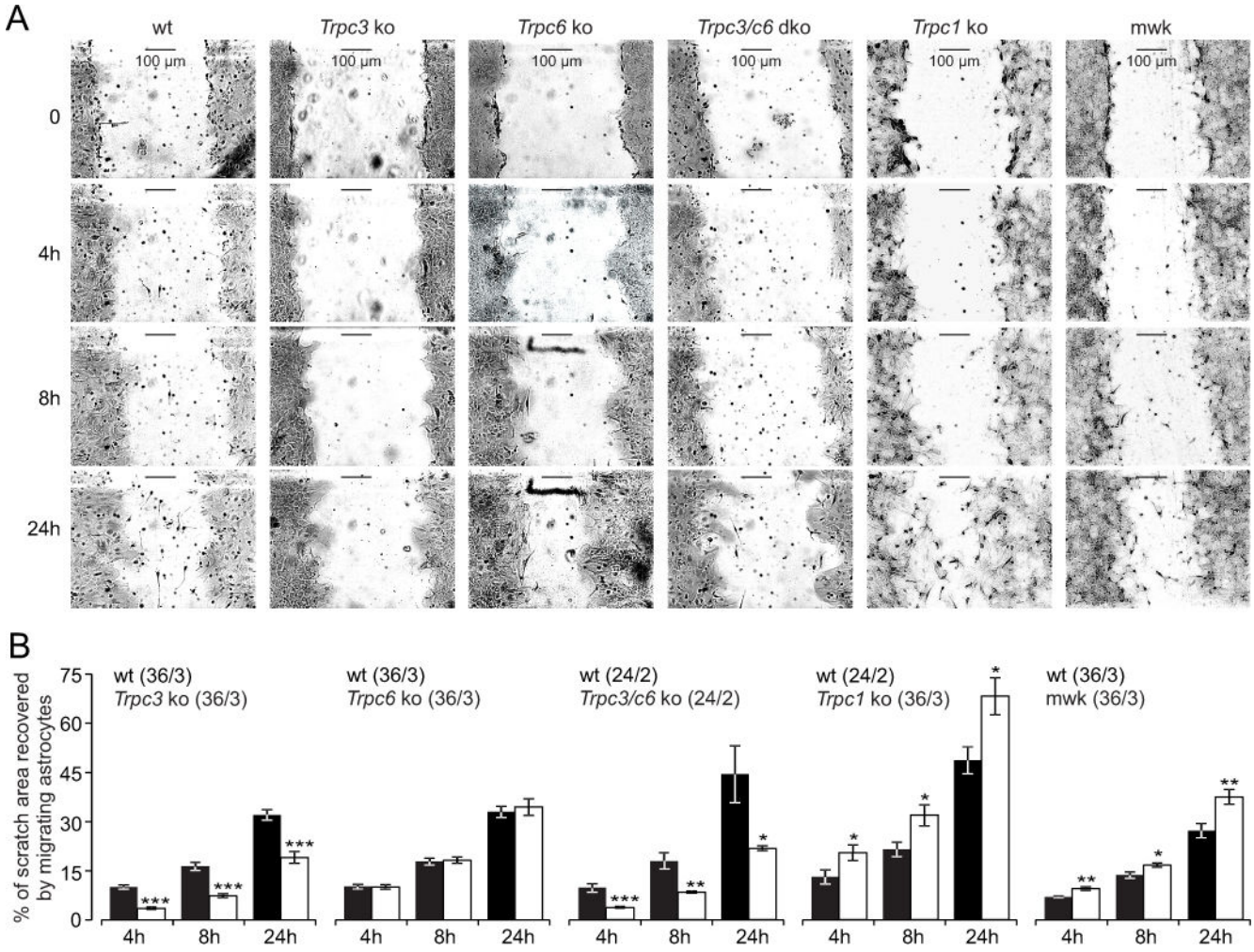

Figure 6. ***In vitro*** **migration of astrocytes depends on** ***Trpc3 and Trpc1***

(**A**) Representative images of scratched areas in cultured astrocytes isolated from wild-type (wt), *Trpc3*$^{-/-}$ (*Trpc3* ko), *Trpc6*$^{-/-}$ (*Trpc6* ko), *Trpc3*$^{-/-}$/*c6*$^{-/-}$ (*Trpc3/c6* dko), *Trpc1*$^{-/-}$ (*Trpc*1 ko) and heterozygous TRPC3$_{T635A}$ mutant (mwk) mice directly (0 h) and 4, 8 and 24 hours after scratching. (**B**) Data as in A, plotted as percentage of scratch area recovered by migrating astrocytes 4, 8 and 24 hours after scratching. Data in B represent means ± S.E.M. (n, number of experiments from x, number of cultures (n/x)). Asterisks assign the significant differences compared to the corresponding wt at the same hour (* P<0.05, ** P<0.01, *** P<0.001).

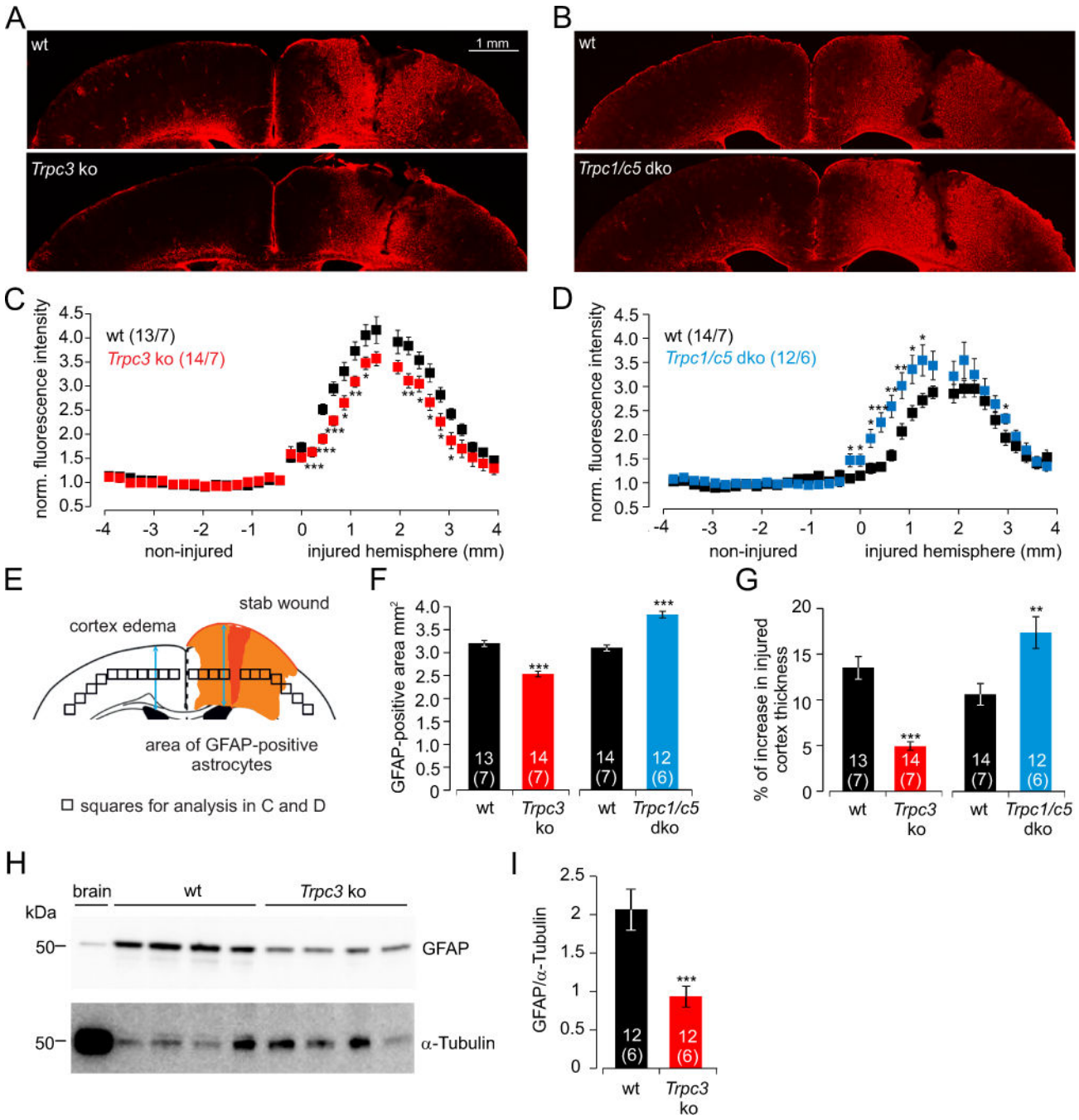

Figure 7. Distribution of reactive astrocytes and cortical edema after brain injury in wild-type, *Trpc3*$^{-/-}$ and *Trpc1*$^{-/-}$ *mice*

(**A**, **B**) Fluorescence images of GFAP (red) -stained brain slices after cortical stab wound injury in wild-type (wt, A, B, top) and *Trpc3*$^{-/-}$ (*Trpc3* ko, A, bottom) and *Trpc1*$^{-/-}$/*Trpc5*$^{-/-}$ (*Trpc1/c5* dko, B, bottom) mice. Since *Trpc5* was not detectable in the cortical astrocytes (Figure 1A and Supplementary Figure 2) we regarded the *Trpc1*$^{-/-}$/*Trpc5*$^{-/-}$ mice as single *Trpc1*$^{-/-}$ mice in respect of the astrocytes. (**C**, **D**) Analysis of the distribution of reactive astrocytes (GFAP-staining) after stab wound injury in *Trpc3*$^{-/-}$ (*Trpc3* ko, C) and *Trpc1*$^{-/-}$/*Trpc5*$^{-/-}$ (*Trpc1/c5* dko, D) mice and the corresponding wild-types. The mean

fluorescence intensity in the squares along the cortex were measured, and normalized to the non-injured hemisphere. The scheme in (**E**) represents the brain slice and symbolizes the location of the squares analyzed in C and D. (**F**, **G**) Summary of the GFAP-stained area as measure for reactive astrocytes (F) and the cortical edema (percentage of increase in the injured cortex thickness, G) after cortical stab wound injury in *Trpc3*$^{-/-}$ (*Trpc3* ko) and *Trpc1*$^{-/-}$/*Trpc5*$^{-/-}$ (*Trpc1/c5* dko) mice and in the corresponding wild-types. Data represent means ± S.E.M. of n, number of analyzed brain slices and x, number of stab wound experiments i.e. x, number of mice (n/x). (**H, I**) Immunoblot of GFAP (top) and α-tubulin (bottom) in lysates from non-injured wild-type brain (lane 1, brain) and from injured hemispheres extracted from the brain slices (see A) of 4 wild-type (lane 2–5) and 4 *Trpc3*$^{-/-}$ mice (lane 6–9; H). Quantification of intensity of GFAP protein stain normalized to the corresponding α-tubulin intensity from background subtracted blots (I, data represent means ± S.E.M. of 12 lanes from lysates from brain slices of 6 wild-type and 6 *Trpc3*$^{-/-}$ animals). Significant differences of *Trpc3*$^{-/-}$ and *Trpc1*$^{-/-}$ compared to the corresponding wild-types are marked with asterisks (* P<0.05, ** P<0.01, *** P<0.001).

Table 1

Oligodesoxynucleotid primer pairs used for PCR

Trpc1	171 bp	5′-TAA AGA TTT GCT CGC ACA AGC CC-3′ and 5′-TTT GAC TGG GAG ACA AAC TCC TTC TGG-3′
Trpc2	173 bp	5′-TCT GCC AGC TCA CGA ATC GC-3′ and 5′-TTT CGT TGA AAT TGC CTA GCT TCT CG-3′
Trpc3	198 bp	5′-CAG CAT TCT CAA TCA GCC AAC ACG-3′ and 5′-AAG ATG GCT AAT TCC TCC GTC GC-3′
Trpc4	168 bp	5′-TGA GAA GGA AGC CAG AAA GCT TCG-3′ and 5′-CCT TAA CAT TCT CCT CCG TCA AGC C-3′
Trpc5	168 bp	5′-GTG GGC GAT GCA TTA CTC TAC GC-3′ and 5′-GTG GGC TGC CAA CAT AAT GGG-3′
Trpc6	197 bp	5′-TCC AGG AAA TTG AGG ATG ATG CG-3′ and 5′-TTG GAA GCC TTG CTT TTG ACC C-3′
Trpc7	152 bp	5′-AGG CCA AAC GCT GTG AAA ACG-3′ and 5′-GTC AAC GGG GGA CAT AAA AGT TAT TGG-3′
Hprt	160 bp	5′-GTC AAC GGG GGA CAT AAA AGT TAT TGG-3′ and 5′-GCT TGC AAC CTT AAC CAT TTT GGG-3′
Trpc1 full-length	2880 bp	5′- [Phos] GAT GAC GTG AGG AGA AAG CC-3′ and 5′- [Phos] TTA ATT TCT TGG ATA AAA CAT AGC-3′
Trpc3 full-length	2733 bp	5′- [Phos] ATG TCC ACC AAG GTC AAG AAG-3′ and 5′- [Phos] TCA CTC ACA TCT CAG CAC ACT G -3′

Table 2

Genes downregulated in astrocytes from *Trpc3*$^{-/-}$ mice compared to expression levels in astrocytes from wild-type mice. Calculated from the means of microarray analysis from three independent cultures each.

Genes	Fold change	Related function	Reference
Enah	−1.51	migration, remodeling of actin cytoskeleton	(Kwiatkowski, Gertler, & Loureiro, 2003)
Eif2s2	−1.52	proliferation	(Gatza, Silva, Parker, Fan, & Perou, 2014)
Odc1	−1.53	proliferation	(Loikkanen, Lin, Railo, Pajunen, & Vainio, 2005)
Eepd1	−1.55	proliferation	(Chun et al., 2016)
Gdf15	−1.58	proliferation	(Duong Van Huyen et al., 2008)
Twist	−1.62	proliferation, migration transcription factor	(Lee & Yutzey, 2011)
Rfx3	−1.86	transcription factor	(Ait-Lounis et al., 2010)
Sox4	−2.69	proliferation, transcription factor	(Bhattaram et al., 2010)

Ait-Lounis, A., Bonal, C., Seguin-Estevez, Q., Schmid, C. D., Bucher, P., Herrera, P. L., … Reith, W. (2010). The transcription factor Rfx3 regulates beta-cell differentiation, function, and glucokinase expression. *Diabetes, 59*(7), 1674–1685. doi:10.2337/db09-0986

Bhattaram, P., Penzo-Mendez, A., Sock, E., Colmenares, C., Kaneko, K. J., Vassilev, A., … Lefebvre, V. (2010). Organogenesis relies on SoxC transcription factors for the survival of neural and mesenchymal progenitors. *Nat Commun, 1*, 9. doi:10.1038/ncomms1008

Chun, C., Wu, Y., Lee, S. H., Williamson, E. A., Reinert, B. L., Jaiswal, A. S., … Hromas, R. A. (2016). The homologous recombination component EEPD1 is required for genome stability in response to developmental stress of vertebrate embryogenesis. *Cell Cycle, 15*(7), 957–962. doi:10.1080/15384101.2016.1151585

Duong Van Huyen, J. P., Cheval, L., Bloch-Faure, M., Belair, M. F., Heudes, D., Bruneval, P., & Doucet, A. (2008). GDF15 triggers homeostatic proliferation of acid-secreting collecting duct cells. *J Am Soc Nephrol, 19*(10), 1965–1974. doi:10.1681/ASN.2007070781

Gatza, M. L., Silva, G. O., Parker, J. S., Fan, C., & Perou, C. M. (2014). An integrated genomics approach identifies drivers of proliferation in luminal-subtype human breast cancer. *Nat Genet, 46*(10), 1051–1059. doi:10.1038/ng.3073

Kwiatkowski, A. V., Gertler, F. B., & Loureiro, J. J. (2003). Function and regulation of Ena/VASP proteins. *Trends Cell Biol, 13*(7), 386–392.

Lee, M. P., & Yutzey, K. E. (2011). Twist1 directly regulates genes that promote cell proliferation and migration in developing heart valves. *PLoS One, 6*(12), e29758. doi:10.1371/journal.pone.0029758

Loikkanen, I., Lin, Y., Railo, A., Pajunen, A., & Vainio, S. (2005). Polyamines are involved in murine kidney development controlling expression of c-ret, E-cadherin, and Pax2/8 genes. *Differentiation, 73*(6), 303–312. doi:10.1111/j.1432–0436.2005.00036.x